Clays and Clay Minerals, Vol. 68, No. 6:544–552, 2020

INFLUENCE OF THE PRECURSOR AND THE TEMPERATURE OF SYNTHESIS ON THE STRUCTURE OF SAPONITE

Sebastian Meyer[1,2], Simona Bennici[1], Cyril Vaulot[1], Séverinne Rigolet[1], and Liva Dzene[1]*

[1]Institut de Science des Matériaux de Mulhouse (IS2M) CNRS UMR 7361, Université de Haute-Alsace, Université de Strasbourg, 3b rue Alfred Werner, 68093 Mulhouse Cedex, France
[2]Metallic Biomaterials, Helmholtz-Zentrum Geesthacht, Max-Planck-Str. 1, 21502 Geesthacht, Germany

Abstract—Several procedures for hydrothermal synthesis of saponite can be found in the literature. They differ in terms of the preparation conditions of the precursor and of the synthesis temperature. The objective of the present study was to investigate how these two parameters influence the structure of the final synthesis product. The precursor was prepared from $Mg(NO_3)_2$, $Al(NO_3)_3$, and Na_4SiO_4 in three different ways: as a gel, a dried gel, and a calcined gel. The influence of the synthesis temperature on the structure of saponite was investigated in the range 90–200°C. The results showed that the use of a calcined precursor yielded a single mineral phase, saponite, with up to 90% aluminum in tetrahedral configuration. In comparison, the use of a gel precursor resulted in a product with only 60% aluminum in the tetrahedral configuration. The synthesis temperature had no significant effect on the saponite structure. The reported synthesis method showed the possibility of obtaining saponite with superior characteristics, in terms of crystallinity, surface acidity, and thermal stability compared to the natural mineral, even at 90°C, and thus with greater potential for industrial application.

Keywords—Minerals · Nanoclay · Precursor · Saponite · Synthesis

INTRODUCTION

For solid-state catalysts, the surface and pore characteristics play a decisive role and have been investigated with many different approaches. Mesophase templating allows synthesis of amorphous silica with defined mesoporosity of up to 10 nm (Gleiter 2000). Limitations with respect to this approach include difficulties with large-scale production and the option to functionalize the surface to create catalytically active sites. Zeolites are easy to synthesize, but access by larger molecules to sites located within the pores, which constitute the majority of the sites available because of the large internal surface area, is restricted due to the presence of micropores with a dimension of <0.8 nm. Partial inhibition of crystallization using an excess of grafted organic species can lead to intracrystalline mesoporosity with increased accessibility for active sites (Xue et al. 2012). Saponite clay minerals, with significant anisotropy due to their layered structure, allow better adsorption of more complex molecules on their surfaces. This makes saponite suitable for a wide range of catalytic applications for organic molecules from cracking, isomerization (Vogels et al. 2005), and oxidation (Trujillano et al. 2009) to the Mannich reaction (Gómez-Sanz et al. 2017). In polymer composite materials, saponite nanoparticles are used to impart novel properties not noted previously at macro or micro scales (Nathani et al. 2004). Improvements in the mechanical properties and hindrance to diffusion were observed. The particular properties of saponites, such as the large cation exchange capacity (CEC) and significant specific surface area, also make them attractive for application as adsorbents and in wastewater treatment, for example (Marchesi et al. 2020). Their large surface area, thermal stability, and wide availability mean that synthetic and natural saponites are increasingly attractive in research and industry (Zhou et al. 2019; Carniato et al. 2020).

Saponites are 2:1 clay minerals and belong to the smectite group; these minerals consist of layers composed of two tetrahedral silica sheets sandwiching an octahedral sheet. For synthetic saponites, the octahedral sheet can contain various divalent metals, e.g. Mg^{2+}, Ni^{2+}, Zn^{2+}, Co^{2+}, and Fe^{2+} (Decarreau 1981; Trujillano et al. 2011). One of the requirements of materials intended for catalytic use is thermal stability. Thermal stability is found to be greater (stable up to 750°C) in saponites (with Mg^{2+} as the major cation in the octahedral sheet) than in montmorillonites (with Al^{3+} as a major cation in the octahedral sheet), which have a maximum stability temperature of 480°C (Ames and Sand 1958).

In the tetrahedral silica sheet, functional ions such as Al^{3+} can substitute isomorphously for Si^{4+} to create active sites. Si–O–Al groups have shown strong acidic properties as a Lewis site (Aquino et al. 2004; Zhou et al. 2019). In addition, the acid activity of clay minerals is said to be correlated with the tetrahedral surface charge density (Davidtz 1976). A product with a large number of Lewis sites and with significant thermal stability could have a structure with a lot of Al^{3+} substitution in the tetrahedral sheet, i.e. having an Al/Si molar ratio of 0.33. The synthesis of a saponite with so much Al^{3+} was demonstrated by Suquet et al. (1977).

In general, the formation of saponites is possible under a wide range of hydrothermal conditions. Moderate conditions with temperatures between 100 and 575°C and pressures to several kbar are most promising in terms of growth rate, yield, and purity (Kloprogge et al. 1999). The study of Kloprogge

* E-mail address of corresponding author: liva.dzene@uha.fr
DOI: 10.1007/s42860-020-00099-1

and Frost (2000) showed that the increase in synthesis temperature (from 125 to 280°C) resulted in the increase in the crystallinity of ammonium saponites. The chemical composition and, thus, to some extent, the saponite crystal structure, would not be expected to change significantly with increasing temperature, however. To test this hypothesis, saponite synthesis was performed over the temperature range of 90 to 220°C and a detailed characterization of the chemical composition and structure of final synthesis product was performed.

While in nature, the formation of smectites is determined by the availability of elements and their speciation (Christidis and Dunham 1997), in hydrothermal synthesis the most common starting materials are solid phases, such as other aluminosilicates, glasses, and gels, the compositions of which are close to that of the desired clay mineral (Kloprogge et al. 1999). The effect of precursor treatments on the structure of the final synthesis products has not been investigated extensively and, therefore, was a further objective of the present study.

EXPERIMENTAL

Synthesis

Solutions (0.2 M) of magnesium nitrate ($Mg(NO_3)_2 \cdot 6H_2O$) from Sigma Aldrich (India), aluminum nitrate ($Al(NO_3)_3 \cdot 9H_2O$) from Carlo Erba (Val de Reuil, France), and of sodium orthosilicate (Na_4SiO_4) from Alfa Aesar (Karlsruhe, Germany) in distilled water (18.2 MΩ·cm) were prepared. The solutions were mixed in a beaker to form a precursor that had a Mg:Al:Si molar ratio of 1:0.33:1. The precursor was then stirred at room conditions for 3 h to achieve a homogeneous suspension. For the precursor experiments, the suspension was placed into the autoclave directly at this stage (sample labeled 'Gel') followed by the hydrothermal treatment. To reduce the water content, the suspension was dried in an oven at 200°C (sample labeled 'Dried gel'). For the rest of the experiments the dried gel was placed in a crucible and calcined at 450°C (sample labeled 'Calcined gel'). At maximum temperature, the holding time was 1 h after a heating rate of 5°C/min and a cooling rate of <10°C/min afterwards.

For the hydrothermal synthesis, a 0.01 M NaOH solution was prepared using NaOH powder from Sigma Aldrich (St Louis, Missouri, USA) and then added to the ground calcined precursor gel. The autoclave with the suspension was closed securely and placed in an oven for 120 h. The synthesis was conducted at 90, 120, 150, 180, and 200°C. In the autoclave the pressure corresponded to the water pressure at those temperatures. The pH was measured with a Hi2211 pH ORP Meter by Hanna Instruments (Tanneries, France) with two-point calibration at pH = 7 and pH = 10 after the precipitation of the precursor and after the synthesis.

After the synthesis, samples were recovered by centrifugation at 8000 rpm (9946×g) for 10 min, which was followed by washing twice with distilled water and ion exchange with Ca^{2+} using 1 M $CaCl_2$ solution (Carrado et al. 2006). The choice to saturate the samples with Ca^{2+} was driven by practical convenience. Because Ca^{2+}-saturated smectites have a two-water layer hydrate structure over a large relative humidity range (Suquet et al. 1975), such material is less sensitive to relative humidity changes and easier to handle during the various characterization experiments. After ion-exchange and washing, the suspension was dried in an oven at 60°C and ground in a mortar.

X-ray Diffraction of Powder and Oriented Preparations

The ground saponite powder was placed in a backloading sample holder and compacted. The prepared sample was measured using an X'Pert Pro instrument from PANalytical (Malvern, United Kingdom) equipped with an X'Celerator real-time multiple strip detector operating with an angular aperture of 2.12°2θ over the 3–70°2θ range using CuKα radiation with a wavelength of 0.15406 nm. The XRD traces were recorded at room temperature with a step size of 0.017°2θ and a scan time of 4 s per step. The divergence slit, the anti-scatter slit, and the two Soller slits were 0.0625, 0.125, and 2.3°, respectively.

Oriented slides were prepared by placing a droplet of the diluted suspension on a glass slide to evaporate with time. Particles settled by gravity and adopted a preferred orientation parallel to the substrate. For optimal measurement results, 3–20 mg portions of powder were used. The dried slides were then recorded over the 3–35°2θ range with the same scanning parameters as before. To saturate the samples with ethylene glycol, the glass slides were placed in a desiccator with ethylene glycol for 2 days.

Fourier-transform Infrared Spectroscopy

The synthesized saponite was mixed with potassium bromide at a weight ratio of 1:100 and ground with a mortar by hand. The powder was placed in a mold and pressed isostatically at 5 bar for 3 min. The resulting pellets were placed in an oven at 150°C overnight to reduce the water content. The FTIR spectroscopy measurements were conducted using an Equinox 55 instrument from Bruker (Karlsruhe, Germany). The spectrum obtained was the average of 32 measurements with a resolution of 4 cm^{-1}. The software *OPUS* was used to record the spectra and to subtract the references with CO_2 and H_2O contributions.

Nuclear Magnetic Resonance (NMR) Spectroscopy

The ^{27}Al MAS NMR spectra were recorded at room temperature with a Bruker Avance II 400 MHz spectrometer (Wissembourg, France) operating at B_0 = 9.4 Tesla giving a ^{27}Al Larmor frequency of 104.23 MHz, equipped with a Bruker 4 mm double channel probe. All experiments were performed at room temperature in ZrO_2 rotors, with a π/12 radio frequency pulse length of 0.5 μs, a recycle delay of 1 s, and at a spinning rate of 12 kHz. The chemical shifts were referred to external $[Al(H_2O)_6]^{3+}$ in $AlCl_3$ aqueous solution. The decompositions of the spectra were performed using the *DMFit* software (Massiot et al. 2002).

X-ray Fluorescence Spectroscopy

The sample pellet was prepared by applying an isostatic pressure of 5 bar on 200 mg of sample. The Zetium spectrometer from PANalytical (Malvern, United Kingdom) was used

to record the spectra from which the composition in terms of wt.% oxides was determined; the atomic wt.% was then calculated.

Nitrogen Adsorption

A Micromeritics ASAP 2420 instrument (Verneuil en Halatte, France) was used to adsorb nitrogen at the temperature of liquid nitrogen (–196°C). Prior to adsorption, 100–200 mg of sample was outgassed in vacuum at 120°C to remove water adsorbed on the surfaces of the particles. The sample mass after pretreatment was measured, then the sample flask was connected to the device for cooling to –196°C throughout measurement. The specific surface area of the sample was derived by means of the BET method (Brunauer et al. 1938) using the *MicroActive* version 4.01 software. The average mesopore size was derived from the adsorption branch of the isotherm using the Barrett–Joyner–Halenda (BJH) method (Barrett et al. 1951). The micro and mesopore size distributions were derived using density function theory (DFT). The slit and cylinder shapes for oxide surfaces were tested and evaluated by their RMS (root mean square) error of the isotherm fit and by the correct fit between the experimental isotherm and the different modelizations (step-like fits were avoided and the fits were tested in log and linear scales).

Transmission Electron Microscopy

Samples were prepared by dispersing the synthesized saponite powder with ultrasound in chloroform. The resulting suspension was evaporated on a carbon coated copper grid at room temperature leaving homogeneously distributed particles. The device ARM200F from JEOL (Tokyo, Japan) with an acceleration voltage of 200 kV was used to record the images. The software *Digital Micrograph* enabled measurement of the average basal spacing by calculating the mean over 6 to 10 clay mineral layers in a selected area.

RESULTS AND DISCUSSION

Influence of Precursor Preparation on Structure Formation

The pH was 12.7 after 3 h of the gel aging and 12.5 after the hydrothermal synthesis. The XRD powder traces (Fig. 1) of synthesis products using different precursors revealed that typical 2:1 trioctahedral clay mineral planes (020), (200), (150), and (060) could be identified in all three samples. The basal reflection (001) at 5.9°2θ was well defined and symmetrical only for the sample prepared from the calcined gel. It indicated an ordered structure with layer-to-layer distances of ~1.5 nm.

For the samples prepared from gel and dried gel precursors, XRD peaks at 12 (0.75 nm) and 24°2θ (0.36 nm) were observed which corresponded to heterogeneous formation of polymorphs of the kaolinite-serpentine group and chlorites. The peak at 35.7°2θ (2.51 nm) and the two peaks at 59.8°2θ (0.154 nm) and 61.1°2θ (0.151 nm) suggested the presence of a lizardite-like structure. Other phases like chlorites could contribute to a greater amount of octahedral Al, especially for the sample prepared from dried gel precursor. The XRD patterns showed crystalline and single clay mineral saponite formation using the precursor of calcined gel. The product after hydrothermal synthesis then contained a purer crystalline saponite. No characteristic peaks of other aluminum phases such as alumina, gibbsite, or boehmite, or of hydrotalcite-like phases were identified in XRD patterns. The small sharp peak at 29.5°2θ (0.303 nm) corresponded to calcite, an impurity arising from incomplete washing prior to the sample saturation with Ca^{2+}.

FTIR spectroscopy was used to check the results from XRD, with respect to sample crystallinity, and to obtain information about the presence of amorphous aggregates and the type of bonds present in the samples. For all three samples, O–H and Si–O vibration modes, characteristic of clay minerals, could be identified (Fig. 2) (Petit 2006). The large bands at ~3400 cm^{-1} and 1629 cm^{-1} corresponded to the vibration modes of H_2O molecules. The band at 1427 cm^{-1} corresponded to carbonates, an impurity identified also by XRD. The O–H bending mode identified at 651 cm^{-1} was characteristic for tri-octahedral clay minerals (Russell and Fraser 1994).

The region of the O–H stretching vibration mode was rather broad for samples prepared from the gel and dried gel precursors. Two bands at 3718 and 3683 cm^{-1} could be identified clearly for the sample prepared from the calcined precursor; the bands corresponded to Mg_3O–H stretching mode. Bands corresponding to the hydroxyl groups were influenced by the saponite layer charge (Pelletier et al. 2003). The Mg_3O–H peak shifted from 3676 to 3692 cm^{-1} due to bond stretching with increasing tetrahedral Al^{3+} substitutions and the compensating cation. The peak visible at 3683 cm^{-1} and also at 3716 cm^{-1} in our reorded spectra provided extra evidence for Al^{3+} substitutions in the tetrahedral sheet. For the sample prepared from the gel precursor, a band at 3656 cm^{-1} corresponding to the Mg_2AlO–H stretching mode (Petit et al. 2004) was observed. It indicated an important substitution of Al^{3+} for Mg^{2+} in the octahedral sheet. Among the broad zone of the O–H stretching mode, two bands were distinguished for the sample prepared from the dried gel precursor: 3613 and 3553 cm^{-1}. These bands were charateristic of Al_2O–H stretching modes. In particular, the 3553 cm^{-1} band was characteristic of chlorites, which was in agreement with phases identified in the XRD pattern (Russell and Fraser 1994).

In all three samples, bands at 991 and 457 cm^{-1} could be identified clearly as corresponding to Si–O vibration modes. In addition, a band at 692 cm^{-1} could also be identified for the calcined gel sample corresponding to the Si–O vibration mode. The substitution of Al^{3+}-for-Si^{4+} in the tetrahedral sheet is known to shift the Si–O stretching mode band value from 1000 cm^{-1} toward lower values, which corresponds to the present case (991 cm^{-1}). The band at 457 cm^{-1} was attributed by Kloprogge and Frost (2000) to the Si–O bending mode of amorphous silica. In the present case, as no other Si–O modes in this region could be identified clearly and, considering the XRD results, this could then correspond to the Si–O vibration mode belonging to clay minerals. However, the possible presence of amorphous silica cannot be ignored. Indeed, a band at ~569 cm^{-1} was identified for the samples prepared from the gel and dried gel precursors,

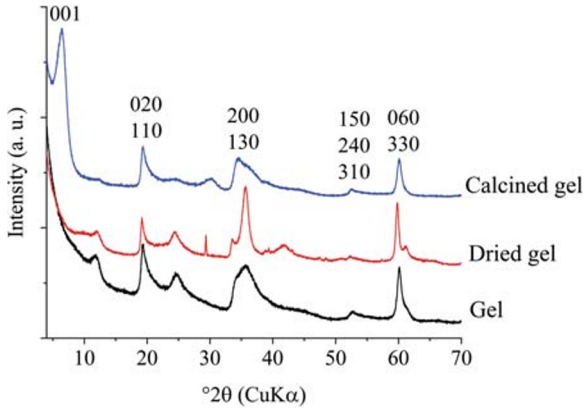

Fig. 1. Powder XRD patterns after hydrothermal synthesis at 200°C using various precursors

reported as belonging to amorphous SiO_2. Finally, all samples contained a band at 823 cm^{-1} attributed to Al–O_4 band vibration, affirming the presence of tetrahedral aluminum. The characteristic bands of alumina were not identified.

The NMR results (Fig. 3) revealed the aluminum resonances for the tetrahedral (^{IV}Al) and octahedral (^{VI}Al) configuration of all precursor types after synthesis. Signals observed at ~60 and ~8 ppm were attributed to ^{IV}Al and ^{VI}Al, respectively (Goodman and Stucki 1984). Using the gel precursor, the Al content was nearly evenly distributed between the octahedral and the two tetrahedral sheets in the final product with ^{IV}Al = 55%. The NMR spectroscopy results were in agreement with the FTIR spectroscopy results, where the Mg_2AlO–H stretching mode was identified, suggesting an important substitution of Al^{3+} for Mg^{2+} in the octahedral sheet. Using the dried and calcinated gel precursors, the tetrahedral aluminum content increased with ^{IV}Al = 80% and ^{IV}Al = 85%, respectively. The NMR results showed a larger amount of octahedral Al in the samples prepared from the gel and dried gel precursors. In agreement with the XRD results, the structure with maximum Al in the tetrahedral position was obtained using the calcined gel as precursor.

In summary, three characterization techniques: XRD, FTIR, and NMR spectroscopies, indicated that the sample prepared from calcined gel precursor gave a better defined structure of saponite with maximum substitution in the tetrahedral sheet than samples prepared using the gel and dried gel precursors. The initial precipitation of precursor was expected to create an homogeneous gel from its constituents (Hamilton and Henderson 1968). The calcination of the precursor removed water and more amorphous regions with a large number of defects were probably created at that stage. Moreover, amorphous and crystalline $Al(OH)_3$-containing compounds could undergo phase transitions at temperatures between 130 and 450°C and were more likely to disappear during the

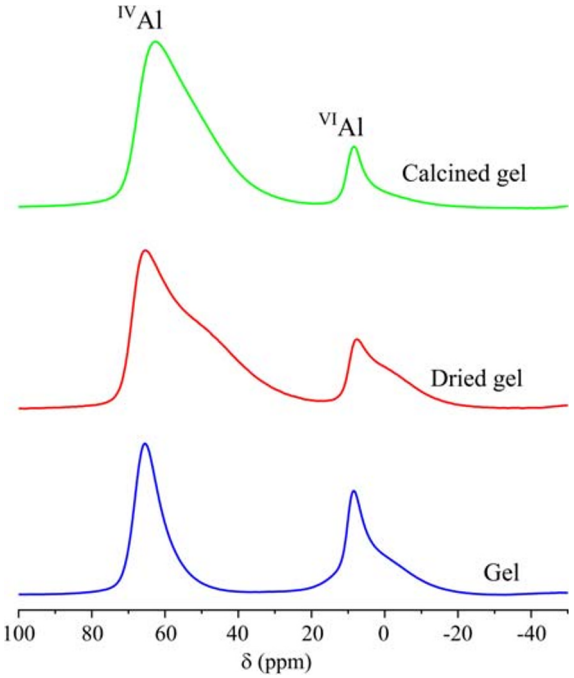

Fig. 3. ^{27}Al MAS NMR spectra of samples synthesized at 200°C with various precursor preparation methods. ^{VI}Al and ^{IV}Al corresponds to

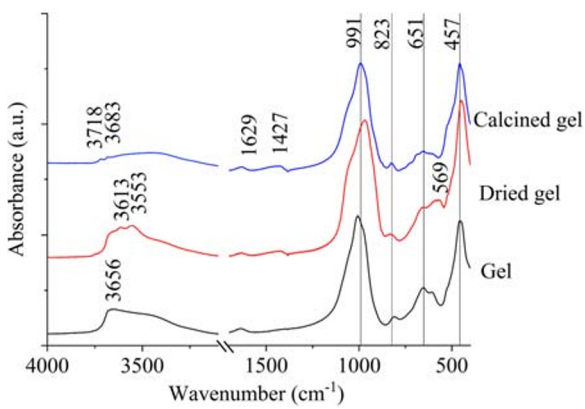

Fig. 2. FTIR spectra of saponite obtained after hydrothermal synthesis at 200°C using various precursors

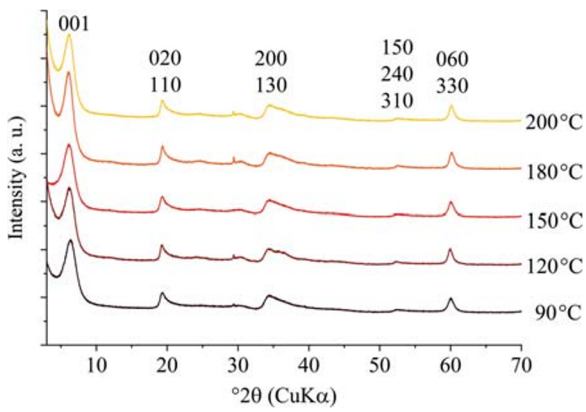

Fig. 4. Powder XRD pattern of synthetic saponite with indexed diffraction planes at various temperatures. d_{001}=1.5 nm and d_{060} = 0.154 nm

calcination of the precursor (Walker 1993; Földvári 2011). During drying, water was evaporated gradually and a very basic environment could have been created locally, thus favoring the formation of tetrahedral Al^{3+}. The powder obtained from the calcined precursor was amorphous and very reactive upon dissolution and subsequent formation of a crystalline phase in hydrothermal synthesis experiments.

Influence of Synthesis Temperature on Structure Formation

The increase in temperature could be expected to enhance the sample crystallinity, as shown by Kloprogge and Frost (2000). The calcined gel precursor was used to synthesize saponites at five different temperatures from 90 to 200°C. The powder XRD pattern (Fig. 4) showed the regular saponite structure to be nearly independent of the synthesis temperature, without crystalline secondary phases. The layer-to-layer distances were between 1.43 and 1.48 nm with a slight tendency to increase with synthesis temperature. Such layer-to-layer distance corresponds to Ca^{2+}-saturated saponite with two layers of water in the interlayer (Suquet et al. 1977).

The swelling property (typical of smectite clay minerals) was assessed using the saturation of oriented preparations with ethylene glycol (Fig. 5). For such preparations, the 001 reflection was pronounced because of the alignment of particles, and shifted its position when saturated with ethylene glycol due to the increase in the layer-to-layer distance. Only a slight shift of ~0.05–0.1 nm was noted and indicated a significant layer charge, as expected. Substitution of Al^{3+}-for-Si^{4+} in the silicate sheets resulted in a more localized charge that had to be compensated by interlayer cations compared to the aluminum substitution in the octahedral sheet, which was compensated over a larger volume by slightly more negatively charged oxygen atoms (Kloprogge et al. 1999). The analysis of oriented slides indicated smaller layer-to-layer distances for the lower synthesis temperatures (90 and 120°C), suggesting a greater interaction between the layers and more pronounced localization of the charge in the tetrahedral sheets. The diffraction peak was broadened with the decrease in temperature, suggesting a smaller particle size and/or more heterogeneous structure.

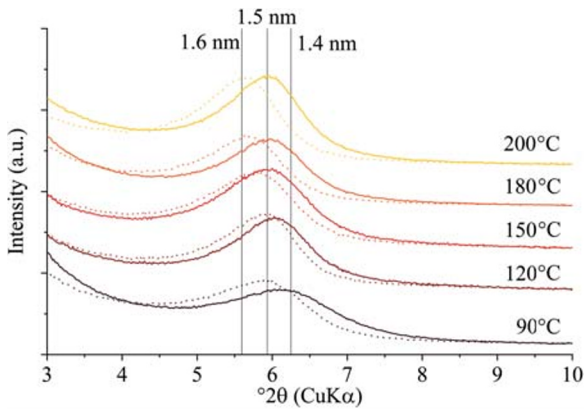

Fig. 5. XRD patterns of 001 reflection of oriented slides at ambient conditions (solid line) and after ethylene glycol saturation (dotted line) with d_{001} indicated above

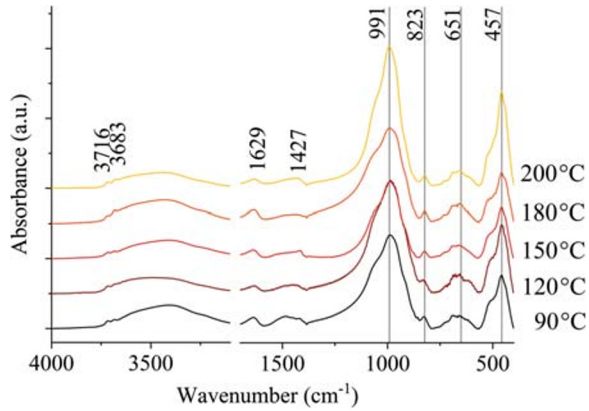

Fig. 6. FTIR spectra of saponite synthesized at various temperatures

For a better insight into the amorphous phases and their bond structure, FTIR spectra were acquired for samples prepared at each synthesis temperature. The bands identified corresponded to bonds in the saponite structure, as discussed previously (Fig. 6). The peak shapes at 991 and 457 cm^{-1} corresponding to Si–O vibration modes indicated a greater crystallinity for synthesis at 200°C. At lower synthesis temperatures, the reduced and broader peaks indicated smaller particle size and/or more heterogeneous structures. Apart from the Si–O vibration bands, the rest of the spectrum seemed to be almost unaffected by the synthesis temperature.

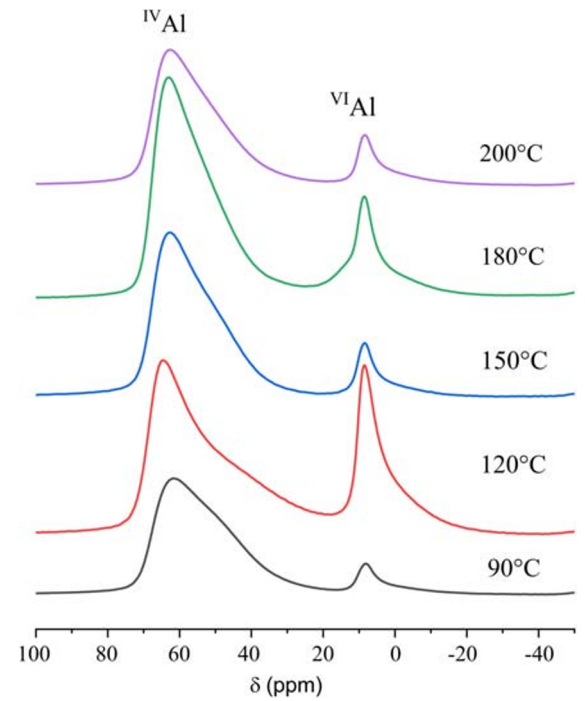

Fig. 7. ^{27}Al MAS NMR spectra of saponite synthesized at various temperatures, indicating aluminum in the octahedral (^{VI}Al) and tetrahedral (^{IV}Al) sheets

Table 1. Element molar ratios obtained by XRF and calculated ratio of tetrahedral aluminum obtained by NMR spectroscopy. Surface area S_{BET} and average pore size calculated from the N_2 method

Synthesis temperature (°C)	Al/Si molar ratio	Mg/Si molar ratio	Ca/Si molar ratio	^{IV}Al by NMR (%)	S_{BET} (m^2/g)	Average pore size (nm)
90	0.42	1.13	0.21	90	172	6.0
120	0.41	0.96	0.20	85	131	8.7
150	0.35	0.99	0.17	90	173	6.2
180	0.36	1.01	0.16	80	113	7.0
200	0.35	0.98	0.17	80	179	6.7

To obtain structural information about the location of aluminum in the structure, NMR spectroscopy measurements were performed (Fig. 7). With the synthesis procedure used, the aluminum content in the tetrahedral sheet was ~80–90%, while the octahedral sheet contained only the small amount remaining. A slight trend toward a larger amount of octahedral Al was observed at high synthesis temperatures (Table 1), in agreement with the trend observed by the XRD experiment performed on oriented slides, which suggested the localization of the charge in the tetrahedral sheet with the decrease of the synthesis temperature. Quantification of the NMR data is rather approximate, however, and a deviation of up to 5–10% should be assumed for interpretation. Even at low synthesis temperatures, however, the vast majority of the substitution by Al took place in the tetrahedral sheet.

The chemical composition of synthesized products was analyzed by XRF spectroscopy. The greatest Al/Si and Ca/Si molar ratios were obtained for samples synthesized at 90 and 120°C (Table 1). The larger amount of interlayer Ca^{2+} correlated with the increased amount of Al substitutions in the structure. Assuming that no other phases were present in significant amounts, and that a slightly larger amount of Al was probably located in the tetrahedral sheets compared to octahedral sheets for samples prepared at a lower synthesis temperature, these results could then also be correlated to the XRD experiments on oriented slides. The analysis of oriented slides led to the hypothesis that for the lowest synthesis temperatures (90 and 120°C) the charge was localized mainly in the tetrahedral sheets. These results were then in good agreement with the chemical composition and NMR results.

The creation of functional groups, such as Lewis acid groups, requires a maximum tetrahedral substitution. Here, the sample synthesized at 90°C, using calcined precursors, showed that many functional groups could be created even at low temperature. In comparison with the study of Kloprogge and Frost (2000), where a shorter synthesis time (3 days instead of 5 days) and a temperature of 280°C were used, a well-defined saponite structure could be obtained, even at lower temperatures.

Nanostructure and Porosity

Although synthesis at 90°C seemed most promising, the FTIR spectroscopy results suggested better homogeneity and/or better crystallinity for the sample synthesized at 200°C. Thus, with XRD and FTIR spectroscopy results alone, how amorphous constituents might be distributed remained unclear.

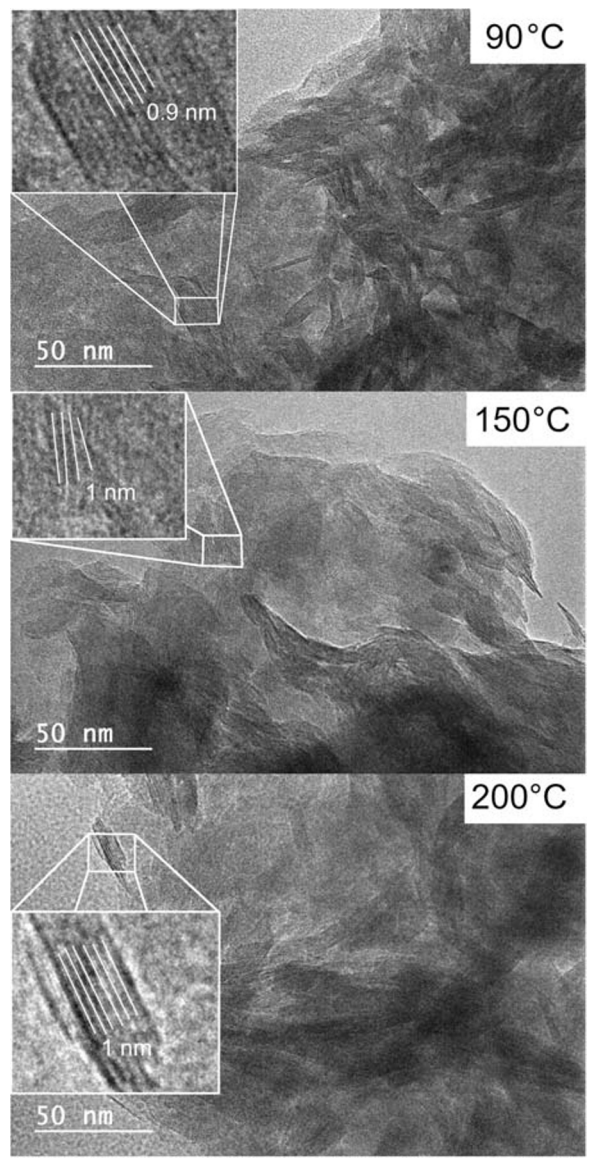

Fig. 8. TEM images of saponite synthesized at various temperatures. Basal spacings derived by lattice-fringe contrast

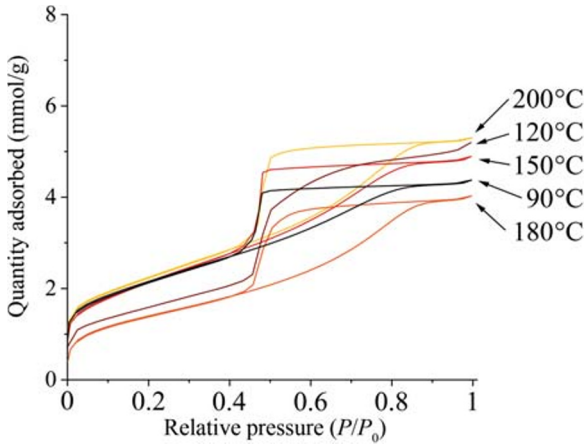

Fig. 9. Isotherms of nitrogen adsorption and desorption for saponites synthesized at various temperatures

TEM observations of samples synthesized at three different temperatures (90, 150, and 200°C) were undertaken to obtain an overview of particle size and shape (Fig. 8). The particle size was estimated visually to be between 50 and 100 nm. The TEM images showed a majority of crystalline regions, which was in agreement with the XRD and FTIR spectroscopy results. No particular difference, in terms of particle size and presence of amorphous aggregates, was observed between samples synthesized at different temperatures. Thus, the slight differences revealed by the XRD and FTIR spectroscopy analysis of oriented slides among the various samples could be due to the inhomogeneity of structure in terms of Al distribution in the structure, which increased with decreasing temperature. In the TEM images, the layer fringe contrast was used to approximate the basal spacing. In all locations chosen, the values were between 0.9 and 1.1 nm. This was considerably smaller than the 1.4–1.5 nm obtained by means of powder XRD. This was due to the removal of interlayer water in the ultra-high vacuum. Note that the estimation of basal spacing was only approximate due to the unknown exact orientation angle of the layers.

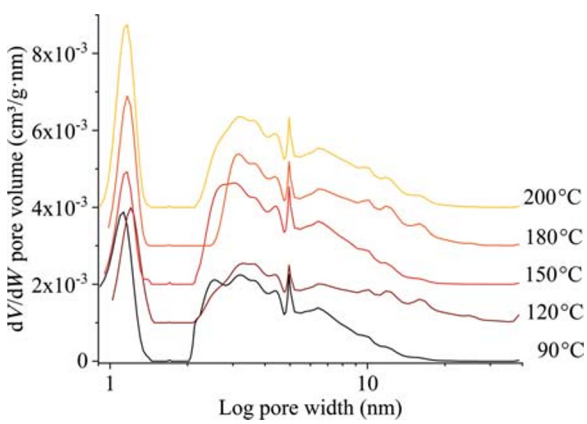

Fig. 10. Pore-size distribution derived from the adsorption isotherm with the DFT method assuming cylindrical pores on an oxide surface with regularization of 0.1

Nitrogen adsorption measurements (Fig. 9) provided additional insight into the microstructure of the samples, giving information about the accessible surface area, pore volume, pore shape, and pore-size distribution. Adsorption at low relative pressure corresponded to the filling of the microporosity and at higher pressure to the mesoporosity. The specific surface area for each temperature of synthesis, determined by the BET method, was up to 179 m^2/g (Table 1). The samples prepared at 120 and 180°C presented the smallest specific surface area. This did not correlate with the microstructural features investigated earlier and may, therefore, be related to sample preparation prior to acquisition of the isotherms. The analysis of the shape of the isotherms (and of the hysteresis) gave information about the pore shape. The adsorption curve was a type IV and hysteresis was of H2 type, according to IUPAC classification. The hysteresis shape corresponded to ink-bottle shaped cavities, which needed to reach a critical pressure (significantly less than during adsorption) in order to desorb nitrogen. By applying the BJH method, average pore sizes of 6–8.7 nm were obtained (Table 1).

With the t-plot technique, a few micropores were identified. Micropores with a diameter of 1.5 nm were found by Occelli et al. (2002) using the DFT model. The derivative of the pore volume over the pore width calculated by the DFT model was then also applied in this study. Clay minerals are known for their layered structure, which means that a slit-like pore shape with constant height but larger and varying width and length could be expected. However, the overall RMS error of the isotherm fit was significantly less assuming a cylindrical pore shape rather than a slit one. The distribution showed two pore domains (Fig. 10). The micropores were distributed closely around 1.1 nm. For the samples obtained at 120 and 180°C, almost no micropores could be found by DFT. No clear trend in the pore size was observable with increasing synthesis temperature. Instead, the pore distribution seemed to remain the same. The mesoporous domain, at >2 nm, was the source of most of the pore volume. On the other hand, micropores contributed to the increase in surface area and their absence in these two samples explained the smaller BET specific surface area measured. If they exist, pillars between the layers could result in more cylindrical shapes, but such structures have not yet been revealed by XRD, FTIR, or TEM, so they can be excluded. Application of a cylindrical pore shape, however, offered a better fit with the presence of mesopores, which contributed significantly to the total volume. These observations showed the discrepancy in the application of the various models, as differentiating among various pore shapes is difficult for any given pore dimension. Cylindrical mesopores could probably be created in the intercrystallite spaces formed during aggregation. The pore shape and size distribution did not correlate (or only partially) with the materials' intrinsic properties, such as the charge, therefore, but rather to the preparation steps, such as grinding, sieving, and outgassing.

CONCLUSIONS

In the present study, saponites were synthesized and the influence of the heat treatment of the precursor was shown. Characterization of the synthesized products by XRD and FTIR spectroscopy indicated that an homogeneous powder of saponite (in terms of structure and chemical composition) was obtained using a precursor calcined at 450°C. A larger quantity of aluminum in tetrahedral configuration was measured for this sample, therefore, which may lead to greater thermal stability and more acidic groups which are useful in catalysis. By using the calcined precursor, hydrothermal synthesis performed at low temperature (90°C) enabled a high-purity saponite to be obtained. A synthesis temperature of 200°C resulted in a very similar product, probably presenting a slightly improved homogeneity, but with lower layer charge and consequently less tetrahedral aluminum.

The distribution of mesopores was found to be in the 2–11 nm range, which is promising for access by large organic molecules. Pillaring or acid activation could also further increase the accessible surface area (Kloprogge 1998; Michot et al. 1998; Trombetta et al. 2000). In contrast to montmorillonite, saponite can be modified more easily by acid leaching due to the presence of octahedral magnesium. Such acidic treatments could greatly enhance the microporosity and specific surface area (up to 510 m^2/g) (Vicente et al. 1996; Bisio et al. 2008).

ACKNOWLEDGMENTS

Nitrogen adsorption experiments, and XRD, XRF, NMR, and TEM analyses were performed on the technical platforms of IS2M. The authors are grateful to Laure Michelin, Loïc Vidal, and Habiba Nouali for their contributions. The internship of Sebastian Meyer was funded by IS2M/UHA in the frame of an 'Emerging' project call. The authors are greateful to the reviewers, and to the editors of the journal Joseph W. Stucki and Kevin Murphy for their remarks and corrections, which allowed significant improvement of the quality of the manuscript.

Funding

Funding sources are as stated in the Acknowledgments.

Compliance with Ethical Statements

Conflict of Interest

The authors declare that they have no conflict of interest.

REFERENCES

Ames, L. L., & Sand, L. B. (1958). Factors effecting maximum hydrothermal stability in montmorillonites. *American Mineralogist, 43*, 641–648.

Aquino, A. J. A., Tunega, D., Gerzabek, M. H., & Lischka, H. (2004). Modeling catalytic effects of clay mineral surfaces on peptide bond formation. *Journal of Physical Chemistry B, 108*, 10120–10130.

Barrett, E., Joyner, L., & Halenda, P. (1951). The determination of pore volume and area distributions in porous substances. I. Computations from nitrogen isotherms. *Journal of the American Chemical Society, 73*, 373–380.

Bisio, C., Gatti, G., Boccaleri, E., Marchese, L., Bertinetti, L., & Coluccia, S. (2008). On the acidity of saponite materials: A combined HRTEM, FTIR, and solid-state NMR study. *Langmuir, 24*, 2808–2819.

Brunauer, S., Emmett, P. H., & Teller, E. (1938). Adsorption of gases in multimolecular layers. *Journal of the American Chemical Society, 60*, 309–319.

Carniato, F., Gatti, G., & Bisio, C. (2020). An overview of the recent synthesis and functionalization methods of saponite clay. *New Journal of Chemistry, 44*, 9969–9980.

Carrado, K. A., Decarreau, A., Petit, S., Bergaya, F., & Lagaly, G. (2006). Synthetic clay minerals and purification of natural clays. In F. Bergaya, B. K. G. Theng, & G. Lagaly (Eds.), *Handbook of Clay Science* (pp. 115–139). Amsterdam: Elsevier.

Christidis, G., & Dunham, A. C. (1997). Compositional variations in smectites. Part II: alteration of acidic precursors, a case study from Milos Island, Greece. *Clay Minerals, 32*, 253–270.

Davidtz, J. C. (1976). The acid activity of 2:1 layer silicates. *Journal of Catalysis, 43*, 260–263.

Decarreau, A. (1981). Cristallogenese à basse température de smectites trioctaèdriques par vieillissement de coprécipités silicométalliques. *Comptes rendus des séances de l'Académie des sciences, 292*, 61–64.

Földvári, M. (2011). *Handbook of Thermogravimetric System of Minerals and Its Use in Geological Practice*. Budapest: Geological Institute of Hungary.

Gleiter, H. (2000). Nanostructured materials: basic concepts and microstructure. *Acta Materialia, 48*, 1–29.

Gómez-Sanz, F., Morales-Vargas, M. V., González-Rodríguez, B., Rojas-Cervantes, M. L., & Pérez-Mayoral, E. (2017). Acid clay minerals as eco-friendly and cheap catalysts for the synthesis of β-amino ketones by Mannich reaction. *Applied Clay Science, 143*, 250–257.

Goodman, B. A., & Stucki, J. W. (1984). The use of nuclear magnetic resonance (NMR) for the determination of tetrahedral aluminium in montmorillonite. *Clay Minerals, 19,* 663–667.

Hamilton, D. L., & Henderson, C. M. B. (1968). The preparation of silicate compositions by a gelling method. *Mineralogical Magazine, 36*, 832–838.

Kloprogge, J. T. (1998). Synthesis of smectites and porous pillared clay catalysts: a review. *Journal of Porous Materials, 5*, 5–41.

Kloprogge, J. T., & Frost, R. L. (2000). The effect of synthesis temperature on the FT-Raman and FT-IR spectra of saponites. *Vibrational Spectroscopy, 23*, 119–127.

Kloprogge, J. T., Komarneni, S., & Amonette, J. E. (1999). Synthesis of smectite clay minerals: A critical review. *Clays and Clay Minerals, 47*, 529–554.

Marchesi, S., Carniato, F., Guidotti, M., Botta, M., Marchese, L., & Bisio, C. (2020). Synthetic saponite clays as promising solids for lanthanide ion recovery. *New Journal of Chemistry, 44*, 10033–10041.

Massiot, D., Fayon, F., Capron, M., King, I., Le Calvé, S., Alonso, B., Durand, J.-O., Bujoli, B., Gan, Z., & Hoatson, G. (2002). Modelling one- and two-dimensional solid-state NMR spectra. *Magnetic Resonance in Chemistry, 40*, 70–76.

Michot, L. J., Villiéras, F., Lambert, J. F., Bergaoui, L., Grillet, Y., & Robert, J. L. (1998). Surface heterogeneity in micropores of pillared clays: The limits of classical pore-filling mechanisms. *Journal of Physical Chemistry B, 102*, 3466–3476.

Nathani, H., Dasari, A., & Misra, R. D. K. (2004). On the reduced susceptibility to stress whitening behavior of melt intercalated polybutene-clay nanocomposites during tensile straining. *Acta Materialia, 52*, 3217–3227.

Occelli, M. L., Olivier, J. P., Peridon-Melon, J. A., & Auroux, A. (2002). Surface area, pore volume distribution, and acidity in mesoporous expanded clay catalysts from hybrid density functional theory (DFT) and adsorption microcalorimetry methods. *Langmuir, 18*, 9816–9823.

Pelletier, M., Michot, L. J., Humbert, B., Barrès, O., D'Espinose de la Caillerie, J. B., & Robert, J. L. (2003). Influence of layer charge on the hydroxyl stretching of trioctahedral clay minerals: A vibrational study of synthetic Na- and K-saponites. *American Mineralogist, 88*, 1801–1808.

Petit, S. (2006). Fourier Transform Infrared Spectroscopy. In F. Bergaya, B. K. G. Theng, & G. Lagaly (Eds.), *Handbook of Clay Science* (pp. 909–918). Amsterdam: Elsevier.

Petit, S., Martin, F., Wiewióra, A., De Parseval, P., & Decarreau, A. (2004). Crystal-chemistry of talc: A near infrared (NIR) spectroscopy study. *American Mineralogist, 89*, 319–326.

Russell, J. D., & Fraser, A. R. (1994). Infrared methods. In M. J. Wilson (Ed.), *Clay Mineralogy: Spectroscopic and Chemical Determinative Methods* (pp. 11–67). The Netherlands: Springer, Dordrecht.

Suquet, H., de la Calle, C., & Pezerat, H. (1975). Swelling and structural organization of saponite. *Clays and Clay Minerals*, *23*, 1–9.

Suquet, H., Iiyama, J. T., Kodama, H., & Pezerat, H. (1977). Synthesis and swelling properties of saponites with increasing layer charge. *Clays and Clay Minerals, 25*, 231–242.

Trombetta, M., Busca, G., Lenarda, M., Storaro, L., Ganzerla, R., Piovesan, L., Lopez, A. J., Alcantara-Rodriguez, M., & Rodríguez-Castellón, E. (2000). Solid acid catalysts from clays Evaluation of surface acidity of mono- and bi-pillared smectites by FT-IR spectroscopy measurements, NH3-TPD and catalytic tests. *Applied Catalysis A: General, 193*, 55–69.

Trujillano, R., Vicente, M. A., Rives, V., Korili, S. A., Gil, A., Ciuffi, K. J., & Nassar, E. J. (2009). Preparation, alumina-pillaring and oxidation catalytic performances of synthetic Ni-saponite. *Microporous and Mesoporous Materials, 117*, 309–316.

Trujillano, R., Rico, E., Vicente, M. A., Rives, V., Ciuffi, K. J., Cestari, A., Gil, A., & Korili, S. A. (2011). Rapid microwave-assisted synthesis of saponites and their use as oxidation catalysts. *Applied Clay Science, 53*, 326–330.

Vicente, M. A., Suárez, M., López-González, J. D. D., & Bañares-Muñoz, M. A. (1996). Characterization, surface area, and porosity analyses of the solids obtained by acid leaching of a saponite. *Langmuir, 12*, 566–572.

Vogels, R. J. M. J., Kloprogge, J. T., & Geus, J. W. (2005). Catalytic activity of synthetic saponite clays: Effects of tetrahedral and octahedral composition. *Journal of Catalysis, 231*, 443–452.

Walker, J. R. (1993). Chlorite polytype geothermometry. *Clays and Clay Minerals, 41*, 260–267.

Xue, Z., Ma, J., Zheng, J., Zhang, T., Kang, Y., & Li, R. (2012). Hierarchical structure and catalytic properties of a microspherical zeolite with intracrystalline mesopores. *Acta Materialia, 60*, 5712–5722.

Zhou, C. H., Zhou, Q., Wu, Q. Q., Petit, S., Jiang, X. C., Xia, S. T., Li, C. S., & Yu, W. H. (2019). Modification, hybridization and applications of saponite: An overview. *Applied Clay Science, 168*, 136–154.

(Received 28 April 2020; revised 11 August 2020; AE: Jianxi Zhu)